Special Issue Article

WIND ENGINEERING

Aerodynamic and aeroacoustic behavior of span-wise wavy trailing edge modified SNL 100 m blade

Wind Engineering
2019, Vol. 43(1) 4–25

DOI: 10.1177/0309524X18818646
journals.sagepub.com/home/wie
SAGE

Seung Joon Yang and James D Baeder

Abstract

The aerodynamic and aeroacoustic behaviors of wavy trailing edge modified flatback wind turbine blade have been investigated through numerical simulation. Previous studies have demonstrated aerodynamic and aeroacoustic benefits of the span-wise wavy trailing edge modification on the flatback trailing edge. The previous two-dimensional airfoil test cases have been extended to a complete set of design parametric study. Aerodynamic and aeroacoustic characteristics of the parametric study have been discussed, relying on the wave size, including recently added cases. Furthermore, in the current study, the wavy trailing edge modification has been applied to the Sandia flatback blade called "SNL100-03FB" and tested in rotating blade conditions. Several variations of the wavy trailing edge design have been tested for a range of wind speeds using an overset computation domain. The numerical simulation employs the in-house developed Navier–Stokes solver, OVERTURNS, as well as Graphics Processing Unit (GPU)-accelerated solver, GPURANS3D. Both are hybrid Reynolds Averaged Navier Stokes (RANS)/Large Eddy Simulation (LES) simulation; delayed detached eddy simulation has been used with the Spalart–Allmaras turbulent model and modified $\gamma - \overline{Re}_{\theta} - \overline{SA}$ laminar–turbulent transition model.

Keywords

Span-wise wavy trailing edge, flatback trailing edge, wind energy, delayed detached eddy simulation, trailing edge vortex, aerodynamics, acoustics, SNL100-03 blade, drag reduction, noise reduction

Introduction

Modern truly large-scale (100-plus-meter) wind turbine blades require very high structural reliability, because of their massive scale. To ensure structurally reliable blade design, lighter and slender (shorter chord length) blades must be one of the solutions. Such properties can be achieved by incorporating a thicker airfoil section with a flatback trailing edge, which allows for a shorter blade chord length, primarily applied to the inboard region. However, a flatback trailing edge increases both aerodynamic base drag and acoustic noise caused by blunt trailing edge, primarily due to the periodic Karman vortex shedding at the trailing edge. Previous studies revealed the flow physics of the flatback airfoils, based on wind tunnel tests of certain flatback airfoils (FB3500-1700 and DU97-W300); they concluded that the aerodynamic drag of these airfoils is 5 to 10 times larger compared to the sharp trailing edge airfoils, over a range of angles of attack from 4° to 20° (Baker et al., 2006; Stone et al., 2009). High drag reduces the maximum lift-to-drag ratio of the airfoil and consequently may reduce the efficiency of the wind turbine in the real situation. On the other hand, low-frequency acoustic noise caused by the periodic vortical shedding off of the flatback trailing edge may detract turbines from the desirability of a wind farm as a clean energy source. Because the strong span-wise trailing edge vortical structures are the main reason for the increased drag and noise signatures, a suitable trailing edge modification must be employed to improve the overall aerodynamic and aeroacoustic performances.

Several types of trailing edge modification have been proposed to disintegrate the strong span-wise coherent trailing edge vortex shedding. These modifications employ additional attachment structures such as a split-plate, serrated-plate, or cavities, to break up the span-wise coherent vortex (Van Dam et al., 2008). However, modifying the trailing edge directly is capable of achieving similar disintegration of span-wise coherent vortex structures. On the other hand, varying the

Department of Aerospace Engineering, University of Maryland, College Park, MD, USA

Corresponding author:
Seung Joon Yang, Department of Aerospace Engineering, University of Maryland, College Park, MD 20742, USA.
Email: sjyang@umd.edu

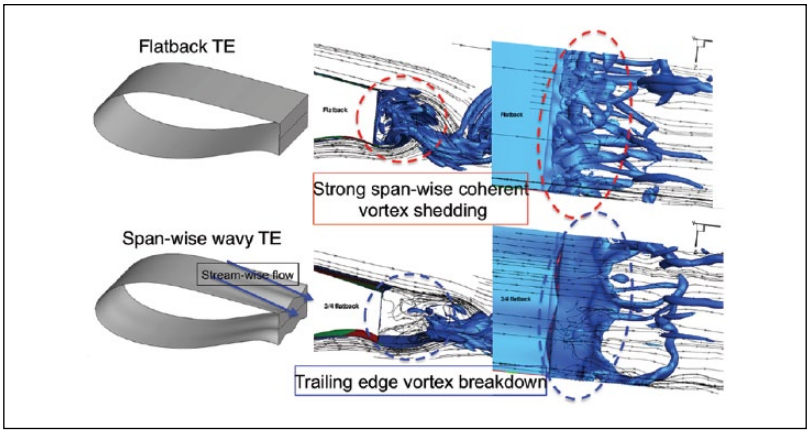

Figure 1. Concept of span-wise wavy trailing edge.

trailing edge thicknesses in the span-wise direction of the blade increases stream-wise flow momentum along the wavy trailing edge, which could potentially dissipate the vortex more effectively than split-plates or serrated-plates. In addition, since the span-wise wavy trailing edge modification requires no mechanical attachment part to the turbine blade, it may make turbine operation maintenances much easier than the other attachment type drag reduction devices. The current study investigates the effects of the span-wise wavy trailing edge modification on the flatback trailing edge version of the Sandia 100 m blade (SNL100-03FB blade), which has the flatback trailing edge applied at the blade inboard (Griffith and Richards, 2014). The current authors performed studies of the span-wise wavy trailing edge airfoils in previous work; it successfully showed aerodynamic drag and noise reductions (Yang and Baeder, 2015). Encouraged by the previous results, in a recent work, the authors modified a section of the SNL100-03 blade with the wavy design and carried out Computational Fluid Dynamics (CFD) simulation over the blade segment, mimicking a wind tunnel blade segment test environment (Yang and Baeder, 2016). Only a part of the inboard section of the SNL100-03 blade has been considered in that simulation. When compared to the unmodified blade segment, the lift was slightly decreased, but the drag was also decreased to a greater extent along the segment.

In the current study, full-scale simulation of the SNL100-03FB blade has been investigated rather than the previous blade segment cases. Updated results of the previous design parametric study have been presented, followed by the current isolated blade simulation results. In particular, flow variations depending on the trailing edge shapes, such as flow separation near the blade inboard and trailing edge vortex shedding, have been presented, followed by discussions of the aerodynamic and aeroacoustic performance. The current studies have been conducted with the use of three-dimensional hybrid RANS/LES. The delayed detached eddy simulation (DDES) with a version of the Spalart–Allmaras (S-A) RANS turbulence model that includes transition model has been used (Medida and Baeder, 2011). In-house three-dimensional Navier–Stokes (N-S) solver, OVERTURNS, and GPU-accelerated solver, GPURANS3D has been used in the current research.

Span-wise wavy trailing edge

The most distinct flow characteristic of flatback airfoil is the Karman-like trailing edge vortex shedding and massive recirculation flow behind the trailing edge. This periodic Karman-like vortex shedding often perturbs strongly the pressure field behind the airfoil and causes acoustic noise, and the strong recirculation flow increases pressure drag of the airfoil. In real three-dimensional configuration of a rotor blade, this flow behavior is even more severe, since the recirculation flow and vortex structures coherently evolve in the span-wise direction. To diminish the negative effect of the span-wise coherent vortex shedding and the recirculation zone, the authors have proposed a span-wise wavy trailing edge design. The design requires variations on the flatback trailing edge shape to disturb growth of the span-wise coherent vortex structures and recirculation zone. The concept of the wavy trailing edge is described in Figure 1. In the figure, strong recirculation flow is clearly formed behind the flatback airfoil and stretches through the airfoil span. In contrast, the strong recirculation flow is eliminated in the span-wise wavy trailing edge case. As described in the figure, more stream-wise momentum of flow is induced to the airfoil behind at each wave and finally breaks up the span-wise coherent vortex structures and strong recirculation flow. Further details of the span-wise wavy trailing edge design, including wave generation method and schematic design, have been presented in the previous publication (Yang and Baeder, 2015).

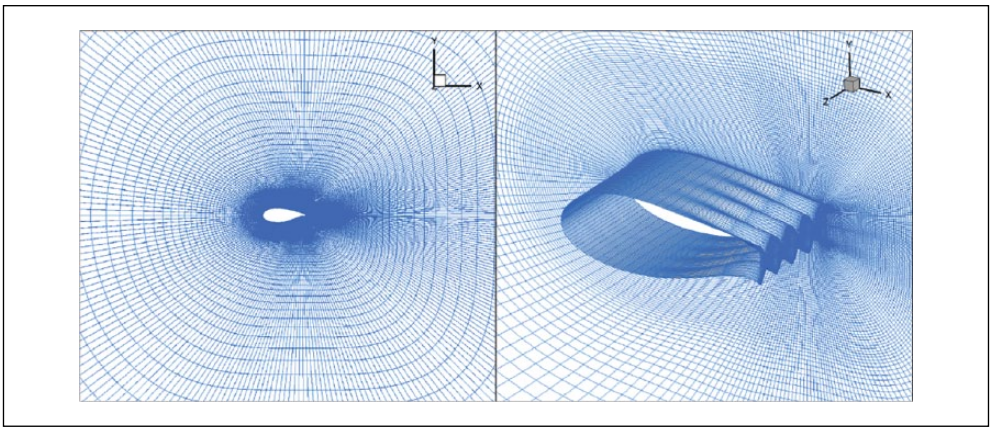

Figure 2. A mesh for the design parametric studies.

Flow solver software

The current study has been performed using the CPU-based parallel N-S solver, OVERTURNS, and the GPU-accelerated N-S solver, GPURANS3D.

The OVERTURNS solver

The OVERTURNS (Overset Transonic Unsteady Rotor Navier–Stokes) is CPU-based, structured, finite-volume, compressible, N-S solver which has been developed at the University of Maryland. In the current study, the third-order accurate Monotonic Upwind Scheme for Conservation Laws (MUSCL) scheme (Van Leer, 1979) with Koren's limiter (Koren, 1993) has been used for spatial reconstruction of primitive variables and second-order accurate implicit Backward Differential Formula (BDF) has been used for time integration. The governing equations are linearized and solved using the Lower-Upper Symmetric Gauss-Seidel (LUSGS) approximate factorization method (Yoon and Jameson, 1988). Dual time-stepping is employed to minimize factorization errors. Roe's approximate Riemann solver (Roe, 1981) is used to evaluate inviscid flux terms and a second-order accurate central difference scheme is used to evaluate viscous flux terms. The one-equation S-A turbulence model (Spalart et al., 2006) combined with the $\gamma - Re_{\theta} - SA$ transition model (Thomas and Baeder, 2013) is used for computing the eddy viscosity field. Turkel's low-Mach preconditioner (Turkel, 1987) is used to improve convergence and accuracy in the low-speed flow regime. Full-scale overset blade rotation cases have been simulated using the OVERTURNS in the current study.

The GPURANS3D solver

The GPURANS3D solver is GPU-accelerated, structured, finite-volume, compressible, N-S solver which has also been developed at the University of Maryland (Thomas and Baeder, 2013). The code has been written using Nvidia CUDA C to exploit the parallelized benefits of the GPU computation. According to benchmark tests, by completely solving the RANS/LES using GPU computation, the computation speed can be accelerated up to more than 50 times faster as compared with typical single-core CPU computations. In this research, the Nvidia Tesla K20m GPU cards in the Deep Thought II High-Performance Computing (HPC) cluster (located in the University of Maryland) have been used. By running on a single GPU card versus running using Message Passing Interface (MPI) on a CPU cluster, there was no domain partitioning required for the current simulations. The GPURANS3D solver has been used for solving the current and previous design parametric study cases. The solver also features DDES with S-A turbulent model and the $\gamma - Re_{\theta} - SA$ laminar–turbulent transition model as well.

Meshes

Meshes for parametric studies

Computational meshes for the design parametric study are constructed using an algebraic O-grid method as shown in Figure 2. Two hundred and seventy-one grid points are used to wrap around in the airfoil surface direction, with 141 grid points set in the normal direction to the surface. Sixty-one grid points are evenly distributed in the span-wise direction as

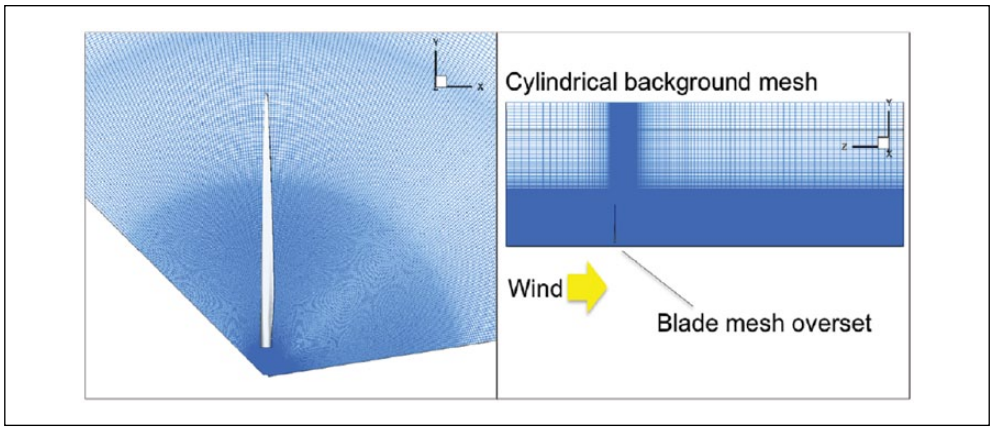

Figure 3. Meshes for the rotating blade cases.

shown in Figure 2. Thus, a total of 2.33 million grid points have been used for each of the airfoil geometries of the parametric cases. Outer physical boundary of the grid system is set as 50 times of airfoil chord length in the normal direction to the airfoil surface and 0.5 times of the chord length in the span-wise direction. Periodic boundary condition is used at both right and left sides of the grid system, thereby effectively simulating an infinite aspect ratio wing. A stretched mesh in the wall-normal direction was used with minimum $y+ \approx 0.8$.

Overset meshes for rotating blade cases

A set of overset meshes has been used for the turbine blade rotation cases. The mesh system consists of a single blade mesh overset to a cylindrical background mesh as presented in Figure 3. The blade mesh has been constructed with a structured O-O topology mesh, dimensions of $269 \times 380 \times 85$ in the wrap-around, span-wise, and wall-normal directions, respectively. The cylindrical background mesh is a structured mesh with dimensions of $184 \times 388 \times 320$ in the azimuthal, radial, and axial directions, and 120° of extent in the azimuthal direction. The mesh also has an extent of four times and eleven times of rotor blade radius in the radial and axial direction, respectively. At the region where the blade inboard is located in the background mesh, meshes have been clustered to a much finer resolution than the other regions to capture the complex vortical flow of the modified turbine blade, and meshes around the blade tip region also have been clustered to be finer to capture the tip vortex traces, but less finer than the inboard mesh clustering. The finest grid spacing in the blade inboard regions of the background mesh is 0.01 of chord length, and 0.05 of chord length near the blade tip.

Design parametric study of size of span-wise wavy trailing edge

Case descriptions

Since the idea of wavy trailing edge modification has not been explored, there are still issues requiring better understanding, such as proper size of the wave and potential structural characteristic changes of the rotor blade or manufacturing difficulties. In the previous study (Yang and Baeder, 2015, 2016), various sizes of wavy trailing edge had been tested, depending on two major design parameters: wave length and depth. A part of case studies in this section had been presented in the previous conference proceedings (Yang and Baeder, 2015, 2016), but new study cases have been added. And expanded result analysis has been included in the current study. It is to be noted that naming notations of the previous modified wavy trailing edge airfoils have been changed in the current work in order to name many different types of modified airfoils in a simpler manner. We believe the new naming notation represents design characteristics of the modified trailing edges, better than the previous notation.

To understand the design parameters, the "FB-3500-1700" flatback airfoil had been modified with different wavy trailing edge patterns. In the previous study, design parameter wave length was four different lengths and labeled with numbers of wave per chord length. Similarly, design parameter wave depth examined for three different depths and labeled with ratio between the minimum thickness and the maximum thickness. For example, if a trailing edge of the flatback airfoil "FB3500" is modified with four waves per one chord length in a span-direction and its minimum trailing edge thickness is 50% of its maximum value, the airfoil is tagged as "4W', "50%t" Thus, the modified airfoil is finally labeled as "FB3500-4W-50%t." Using the notation, 12 individual test cases had been set and presented in Figure 4.

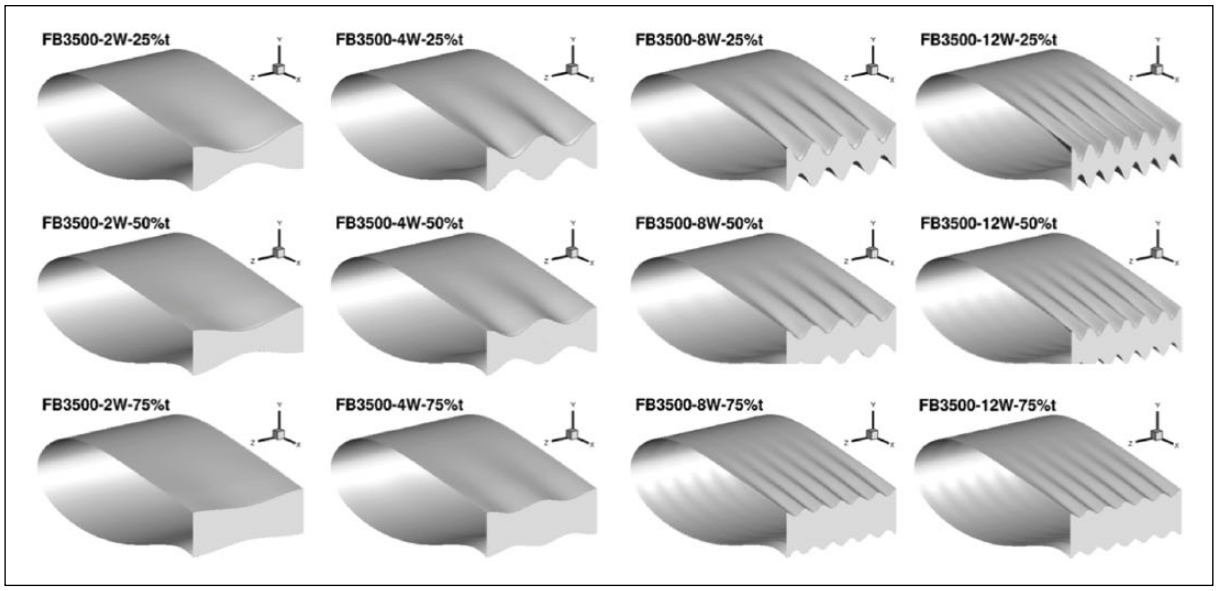

Figure 4. Airfoil geometries of the parametric study - maximum portion of modification.

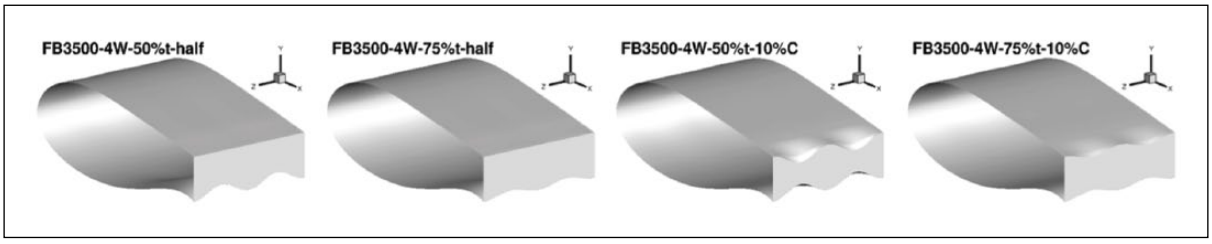

Figure 5. Airfoil geometries of the parametric study - less portion of modification.

In addition to the geometries shown in Figure 4, four additional cases have been studied, considering potential structural characteristic changes on the turbine blade. As shown in Figure 4, our first wavy design modifies an airfoil structure from the trailing edge to near the maximum airfoil thickness location where the main blade spar structure is located. It may bring potential structural characteristic changes to the turbine blade or cause difficulties in the manufacturing process. To avoid the potential structural/manufacturing problems, additional wavy trailing edge cases have been created as presented in Figure 5. All the extended cases are designed with less portion of wavy modification on their trailing edge to avoid any damages to the main spar location. In Figure 5, the first two airfoils from the right side of the figure have been modified their trailing edge only at bottom surfaces of the airfoils and tagged as "half," and the last two have been modified both upper and bottom surfaces of the airfoils but only at the last 10% of the airfoil trailing edge and tagged as "10%C." Along with flow simulation of the described cases, a case of structural simulation has been carried out to test potential structural failure of the wavy trailing edge design.

Aerodynamic and aeroacoustic characteristics

In this section, all the flow simulations have been performed using the GPURANS3D solver with the Deep Thought II HPC clusters at the University of Maryland. For the parametric study cases, flow conditions are flight Mach number 0.3, Reynolds number 666,000, and angle of attack 8°. Here we note that both the original FB-3500-1750 flatback and FB-3500-0050 sharp trailing edge airfoils do not show flow separation at these flow conditions.

After combining the previous cases and newly added cases, we have mapped the aerodynamic performance data for all of the test cases with lift coefficient versus drag coefficient chart, as shown in Figure 6. There are two common characteristics of all the wavy modified cases: (1) the lift coefficient is always less than the original flatback airfoil; (2) the drag coefficient is also always less than the original flatback cases, but larger than the sharp trailing edge airfoil. However, between the cases, the following modified wavy trailing edge airfoils give not too much loss of lift force (less than 6%

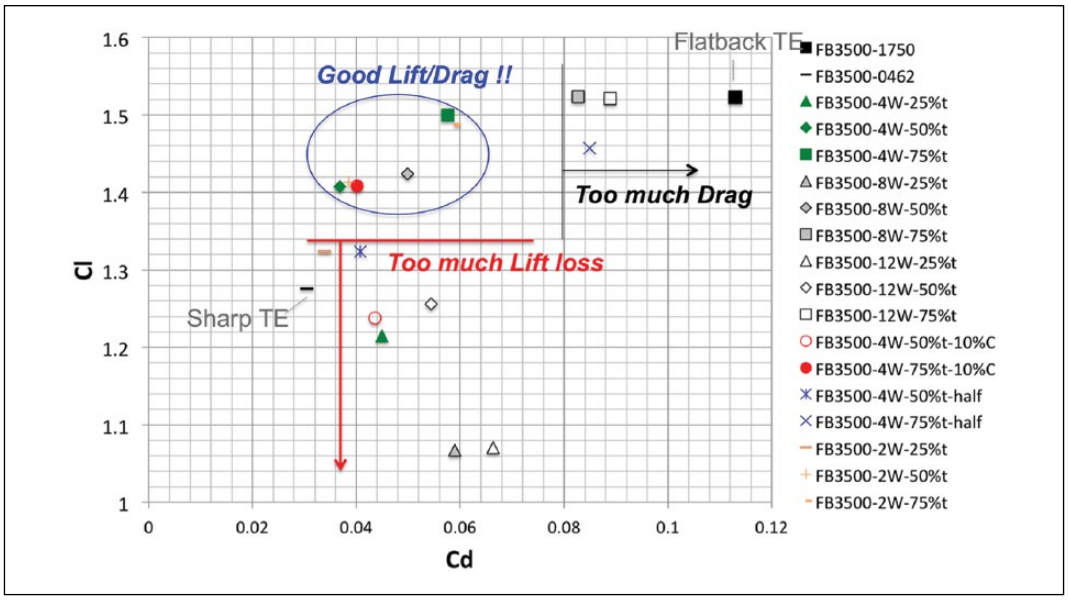

Figure 6. Aerodynamic performance map of the parametric study.

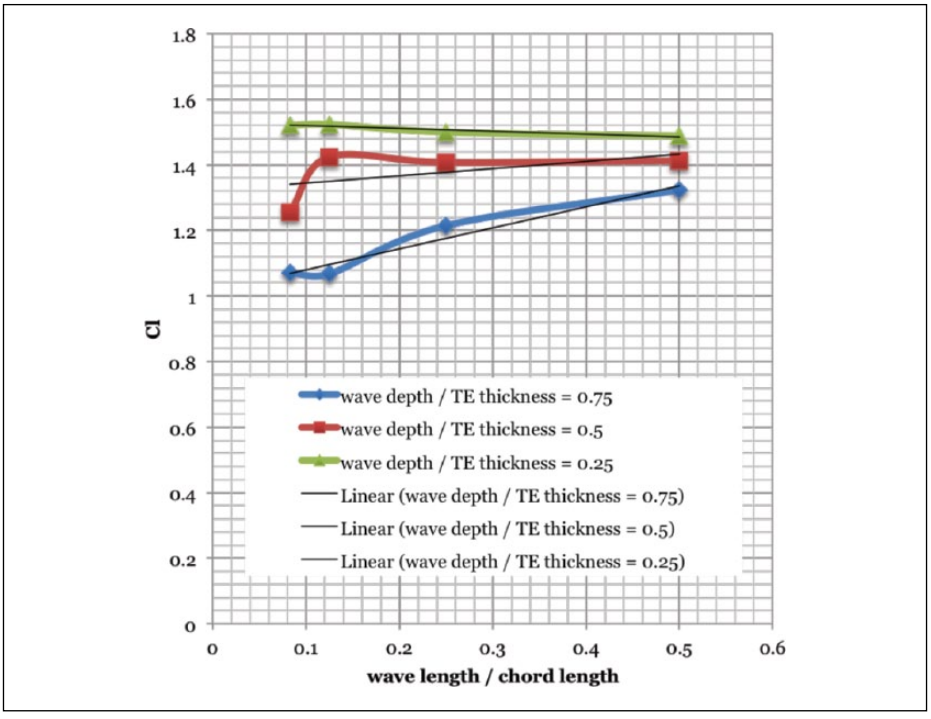

Figure 7. Effect of wave length and depth on the lift force.

of lift loss) as well as large reduction of drag force (up to 66% of drag reduction) indicated inside of circle in the chart: FB3500-2W-75%t, FB3500-2W-50%t, FB3500-4W-75%t, FB3500-4W-50%t, FB3500-4W-50%t-10%C, and FB3500-8W-50%t. These are the ideal design candidates for the investigation, reducing drag as much as possible while maintaining lift close to that of the original flatback airfoil.

To understand why some of designs are successful but the others are not, the aero dynamic results have been plotted with two primary sizing factors: wave depth and length. First, effect of wave size to the airfoil lift has been considered. In Figure 7, lower wave depth/trailing edge thickness as 0.25 (same as airfoil notation "75%t") is not sensitive to lift force with wave length variation. But as the wave depth gets deeper, sensitivity to the lift grows with decrease

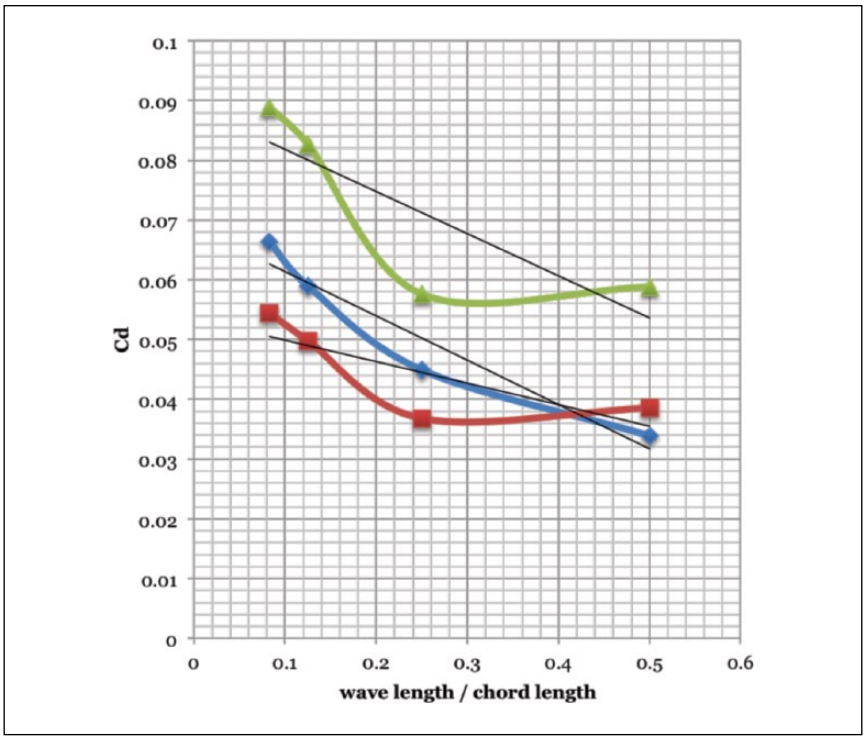

Figure 8. Effect of wave length and depth on the drag force.

of the wave length. The results show if we gouge the trailing edge wave no deeper than the half of trailing edge thickness, the lift of the airfoil does not change much with wave depth and length, unless the wave length is too short (less than 0.12 wave length per chord length). Effect on the drag is more sensitive to both wave length and depth. In Figure 8, drag of the wavy modified airfoils is distinctly different by the wave depth variations. Effect of wave length is also distinct here; the drag values are linearly decreasing from the very short wave length until the wave length is longer than 0.25 wave length per chord length (same as airfoil notation "4W"). However, much longer wave length than 0.25 does not provide further drag reduction as much as 0.25 wave length.

Concluding the results so far, the given flatback airfoil "FB3500-1700" should be modified no deeper than half depth of the trailing edge thickness, no shorter than 0.12 wave length per chord length, so as not to lose lift force of the original airfoil. In the meanwhile, the wave length should be larger than 0.25 wave length per chord length to reduce enough drag force from the original airfoil, but to wave depth, a factor of 0.5 would be the best choice in the current case. Interestingly, loss of lift is linearly increased by increasing the wave depth, but proper wave depth and length will be required to reduce the drag force, depending on the given flatback airfoils. Looking at the Cl, Cd plots in Figures 7 and 8, there is another interesting feature of the wavy modification. We confirmed with flow contour and pressure distributions of the airfoil that loss of the lift force of the wave depth/Trailing Edge (TE) thickness = 0.75 ("25%t") is mostly caused by flow separation just upstream of the modified trailing edge. In this case, the maximum loss of the lift is about 30% of the original blade, but one still gets about 40% reduced drag by breaking the span-wise coherent trailing edge vortex structure. This implies that span-wise coherent vortex structure of the flatback airfoil strongly affects the rise of airfoil pressure drag.

The lift-to-drag ratios have been plotted in Figure 9. The lift-to-drag ratios of FB3500-4W series are much higher, comparing with the other wavy airfoil series, regardless of the wave length. Here we call back the four less portion wavy trailing edge modification. As shown in Figure 6, it shows only the last 10% of trailing edge modified cases ("10%C") are placed at the better locations in the performance map compared to the larger portion wavy modified airfoils with same length and depth. In a sense of the structural concerns of the given modification, modifying blade structures on less portion of the chord are desirable. For the cases, the lift-to-drag ratio envelopes of the larger portion and less portion wavy trailing edge airfoils have been compared in Figure 10. With 75%t wave depth, surprisingly a better aerodynamic performance is achieved with the less portion wavy trailing edge. This is similar aerodynamic performance with the previous best performance case "FB3500-4W-50%t." Besides the aerodynamic characteristics, aeroacoustic characteristics have been analyzed and presented in Figure 11. The worst acoustic behavior of the flatback

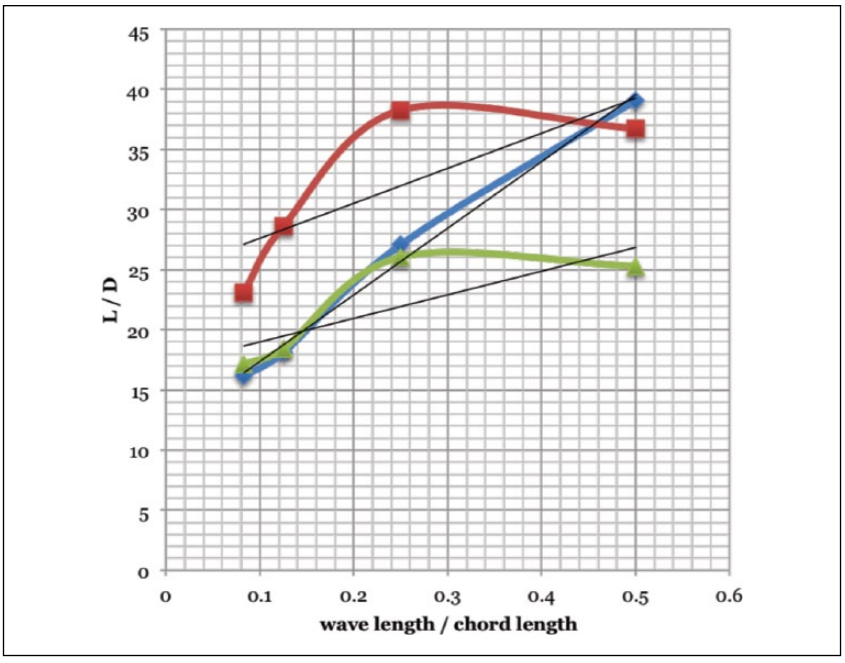

Figure 9. Effect of wave length and depth on the lift/drag ratio.

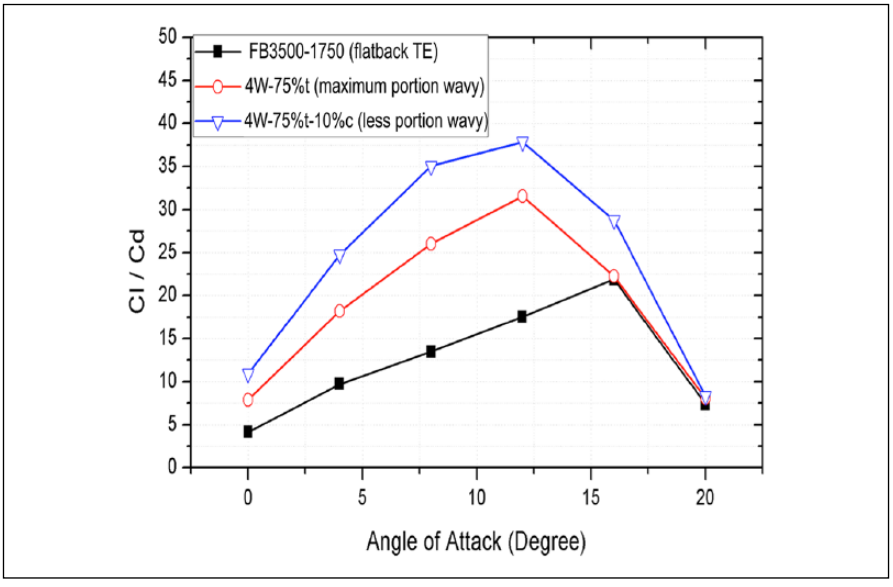

Figure 10. Lift/drag envelopes at a range of angles of attack 0°–20°.

airfoil in this case is the strong tonal noise at low frequency band. Comparing to the large portion modified wavy trailing edge, "FB3500-4W-75%t," the tonal noise of the flatback airfoil has vanished with the less portion modified airfoil, "FB3500-4W-75%t-10%C." This is encouraging to apply the span-wise wavy trailing edge modification to real blade cases, since now we know a small amount of blade structure modification can provide strong variation of the trailing edge vortex structure and reduce the strong tonal noise and the large pressure drag caused by flat trailing edges while minimizing changes of a blade structure.

Structural buckling analysis

Structural effect of the span-wise wavy trailing edge has been discussed in the previous study and explained in this subsection to support the view of potential structural effect of the span-wise wavy modification stated in the previous

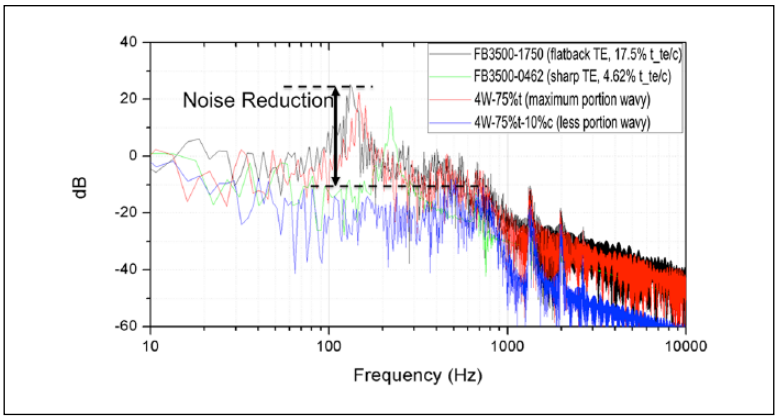

Figure 11. Acoustic behaviors at low frequency band.

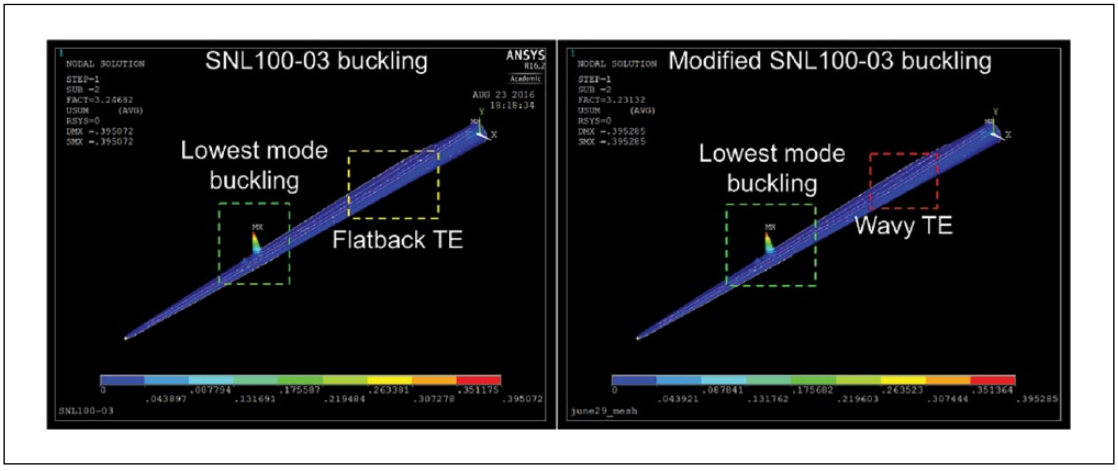

Figure 12. Lowest mode buckling results.

section (Yang and Baeder, 2016). Simple structural analysis, such as maximum deflection test, eigen buckling test had been performed. To compare the original flatback blade and the span-wise modified trailing edge blade, the "SNL100-03FB" and a span-wise wavy modified SNL100-03FB blades had been analyzed. The blade geometries and numerical solver input parameters including material properties had been set up using NuMad software, which had been developed and provided by Sandia National Laboratory (Griffith and Richards, 2014). Aerodyn V15 has been used for generating airloads on the blades; Ansys APDL (Ansys Parametric Design Language) mechanical solver has been used for the eigen buckling simulations. In the results, the maximum deflections were the same on the two blades, as well as the lowest mode buckling. The results of the buckling simulations are shown in Figure 12. For both cases, noticeable buckling response occurs near the outboard of the blade where the third shear web of the blade ends. There is no significant buckling at the wavy modified region. Further details of the buckling analysis had been presented in the previous work (Yang and Baeder, 2016).

Span-wise wavy modified SNL100-03 results

Span-wise modified SNL100-03FB blade

The effect of the span-wise wavy trailing edge modification on the wind turbine blade has been investigated with rotating blade flow conditions. The SNL100-03FB blade designed by the Sandia National Laboratory (Griffith and Richards, 2014) has been selected as a baseline blade in the current study. The design of the SNL100-03FB contains flatback trailing edge within regions of 10%–60% of the blade span. The flatback trailing edge region of the baseline blade has been modified based on the span-wise wavy trailing edge design, "4W-50%t-10%c" in the current section. Details of the modification have been described in Figures 13 to 15. The size (length and depth) of the wave at each span locations has been synchronized with

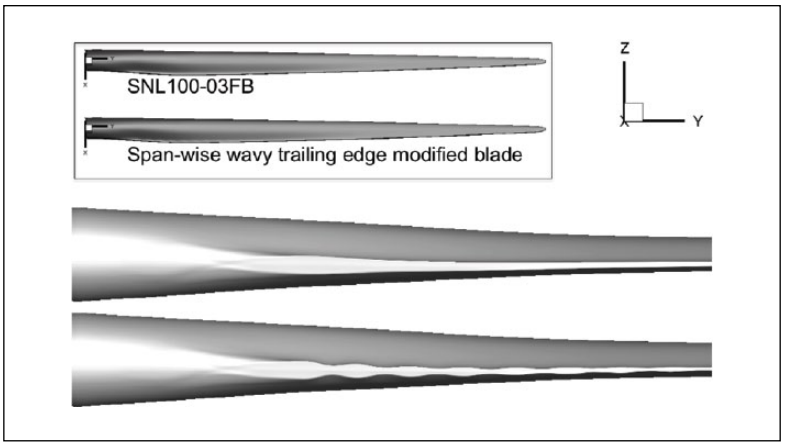

Figure 13. Geometries of the SNL100-03FB and its span-wise wavy trailing edge modification.

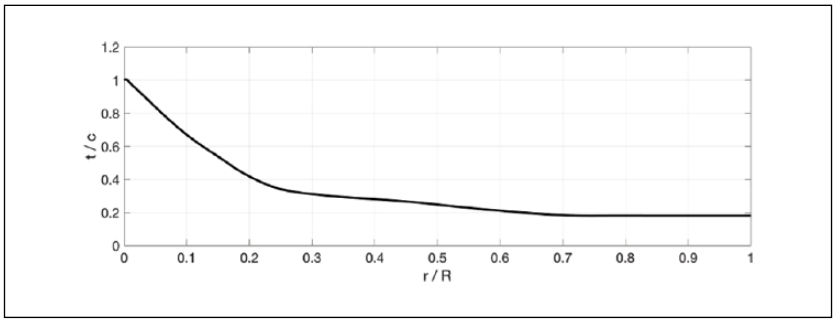

Figure 14. Thickness to chord ratio over the SNL100-03FB blade span.

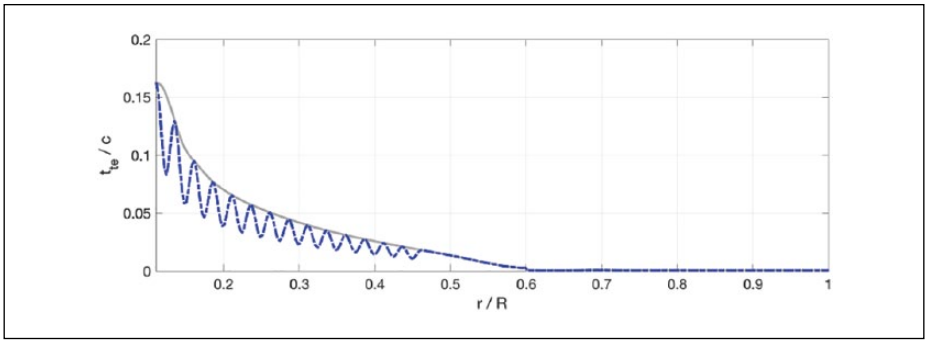

Figure 15. Trailing edge thickness to chord ratio over the SNL100-03FB and the span-wise wavy trailing edge blade.

local chord length and trailing edge thickness of the baseline blade. Based on the previous results of the parametric study, the "4W-50%t-10%c" modification design has been selected. The modification of the wave length "4W" and the wavy depth "50%t" was not very effected on the manner of aerodynamic performance, but it reduced acoustic noise most among the modifications. The portion of modification, "10%c," has been selected to minimize negative effect on the blade structure.

The rotating blade simulation cases in this subsection have been performed with a range of wind speed between 4 and 15 m/s. Blade pitch control begins at wind speeds above 12 m/s, and blade offset distance is 11.3 m from the center of rotation. The other flow conditions are presented in Table 1. Test cases of the current subsection have been performed with the OVERTURNS solver.

The power coefficient of the test cases has been compared with the WTPerf data provided in the Sandia report (Griffith and Richards, 2014). In Figure 16, overall, the power coefficient prediction of the current CFD is comparable to the WTPerf results, although the current CFD has slightly under-predicted. This is a common tendency when comparing

Table 1. Flow conditions of case study.

Wind speed (m/s)	Rotor RPM	Pitch (°)	Re ($\times 10^6$)
4.0	4.638	0.000	3.305
6.0	5.650	0.000	4.025
8.0	6.933	0.000	4.941
10.0	7.157	0.000	5.101
11.3	7.401	0.000	5.273
12.0	7.438	3.231	5.301
13.0	7.438	6.166	5.301
15.0	7.438	10.120	5.301

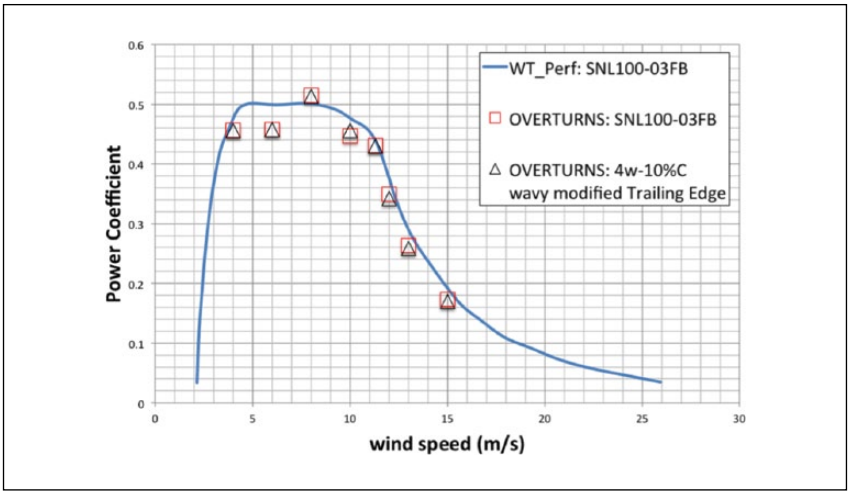

Figure 16. Power coefficient of test cases.

a high-fidelity CFD and low-order BEM (Blade Element Method). Comparing the BEM, the CFD usually can capture unsteady features - such as blade tip vortex and root separation - more realistically. Comparing between the baseline blade and the span-wise trailing edge modified blade, no significant difference has been found at the ranges of lower wind speeds, but the modified blade cases show slight power loss for the blade pitch controlled flow conditions.

To view the details, results at wind speed of 6 m/s (lower speed wind) and 12 m/s (blade pitch controlled) have been compared and reviewed. Overall, thrust and power of the two different wind speed cases are presented in Table 2. As shown in Figure 16, overall power performances between the baseline and modified blades are not significantly different at the low wind speed. However, at the wind speed of 12 m/s, about 2% of thrust loss and power loss has been observed by the trailing edge modification. This might be a small fraction of loss the thrust and power, but if integrated the power generation for a year might not be negligible. Further design trade-off might be interesting between the power loss and noise reduction if a real turbine project employs the span-wise wavy modification. To provide overview of the flow characteristics of the two different blades for different wind speeds, integrated flow contours have been presented in Figures 17 and 18. The iso-vorticity contours of the baseline and modified blades are not very different at wind speed of 6 m/s. At wind speed of 12 m/s, flow near the blade root and inboard of the two blades look different. In the baseline blade case (in the left of Figure 18), the strong vorticity generated only at the root region, up to 0.1 r/R, and grew to the large swirling vortex with strong strength. In contrast, in the modified blade case (in the right of Figure 18), the root vortex generated at more broad region through the blade span and formed vortex swirl with less strength than the baseline blade.

This is also found in the sectional aerodynamic force distribution over the blade span. Figures 19 and 20 present span-wise distributions of axial (out of plane) and chord-wise (in plane) propulsive force generations over the blade, respectively. Looking at the area where the forces are very similar in the figures, in both cases of wind speed of 6 and 12 m/s, the force generation from the mid-span to the tip looks identical between the baseline and modified blade since there is no modification at that region. However, there is still very similar amount of forces generated from the mid-span to around 0.3 r/R inboard for all of the cases. Before testing the blade, we assumed that region also still is flatback effect dominated as much as near the root region, therefore expected at least some span-wise vortex shedding.

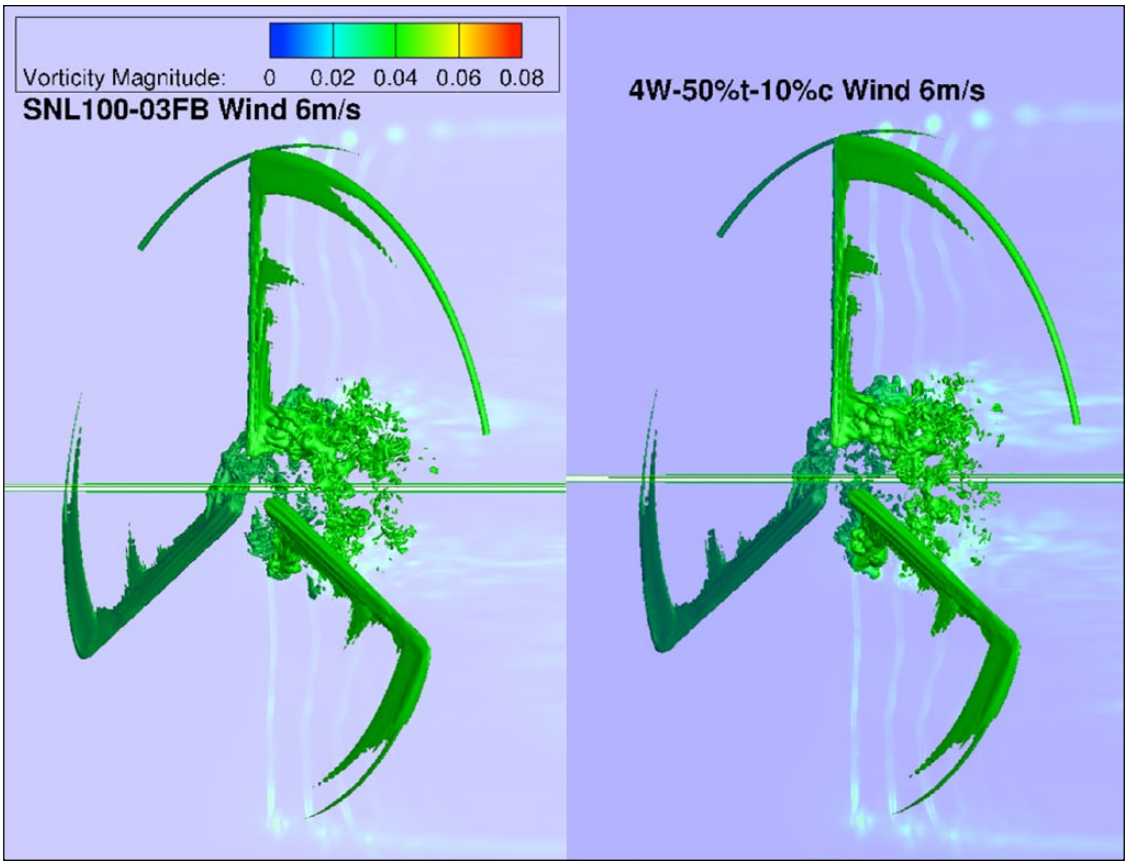

Figure 17. Vorticity magnitude contours at wind speed of 6 m/s.

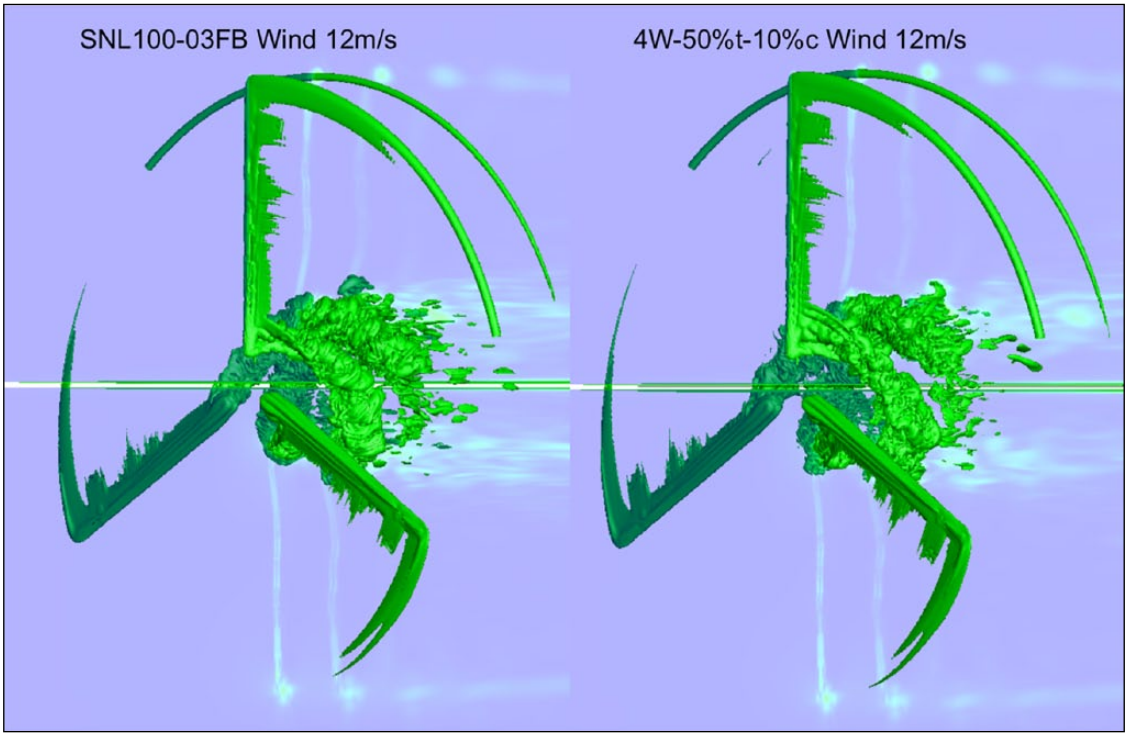

Figure 18. Vorticity magnitude contours at wind speed of 12 m/s.

Table 2. Comparisons of the integrated turbine performance between the baseline and 4W-50%t-10%c modified blade.

Modification type	Thrust (kN)	ΔT	Power (MW)	ΔP
At wind speed of 6.0 m/s				
SNL100-03FB	701.18	N/A	2.339	N/A
4W-50%t-10%c	699.26	−0.27%	2.338	−0.04%
At wind speed of 12.0 m/s				
SNL100-03FB	1578.3	N/A	14.28	N/A
4W-50%t-10%c	1547.1	−2.0%	13.97	−2.2%

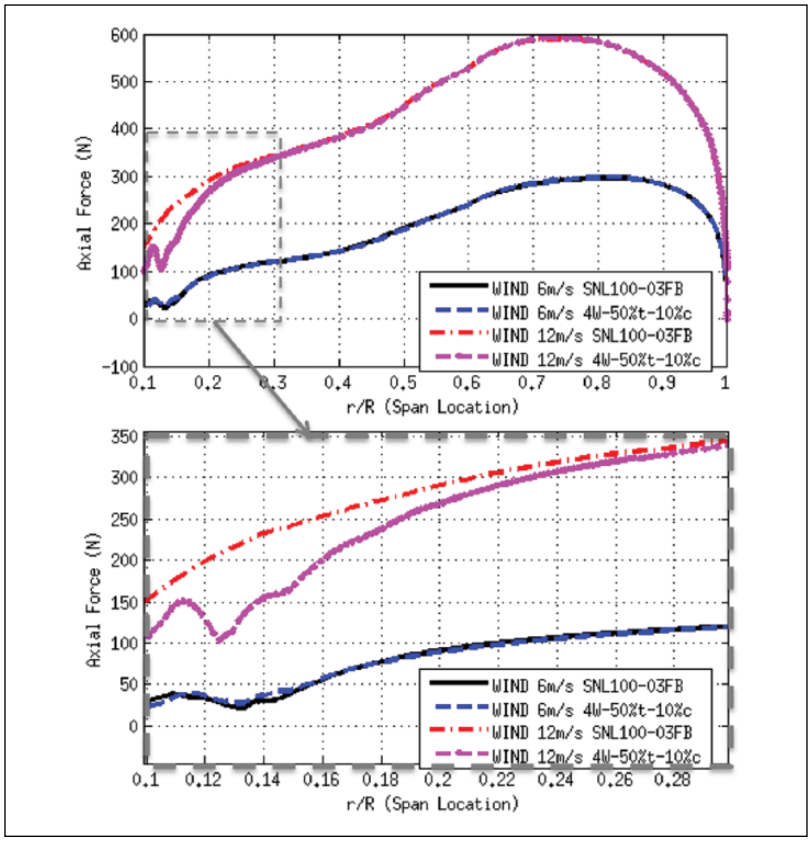

Figure 19. Axial force distribution (out of plane) over the blade span.

However, it was found that strong vortex shedding is not present at the mid-span in the actual simulations, since the trailing edge thickness in the region is not thick enough as compared to the near root regions. In this flow condition, no trailing edge modification is required for the flatback trailing edge. The span location of 0.1 r/R is a geometric transition region between the cylindrical geometry of the blade root and the airfoil geometries. At the wind speed of 6 m/s, the force generation is not very different between the baseline and modified blade, but the in-plane force has been increased slightly in the region between 0.1 r/R and 0.14 r/R. The iso-vorticity contours are illustrated in Figure 21. The vortex structures again are not very different, but much smaller details of the vortex structure have been observed in the modified blade.

Furthermore, differences have been observed at the region between 0.1 r/R and 0.3 r/R of blade span at the wind speed of 12 m/s. In this region at that wind speed, the force generations of the modified blade are reduced compared to the baseline case. Cause of this loss of the forces can be found in the vorticity distribution at the region, as shown in Figure 22. In Figure 22, in the iso-vorticity contour of the modified blade, two of the slightly smaller scale vortex structures caused by flow separation have been observed more broadly at the region, compared to the sole larger scale of vortex structure observed in the baseline case. Thus, broad flow separation caused by the wavy trailing edge decreases the thrust, particularly at the location where the second vortex structure (at 0.13 r/R) exists (Figure 19 and 20).

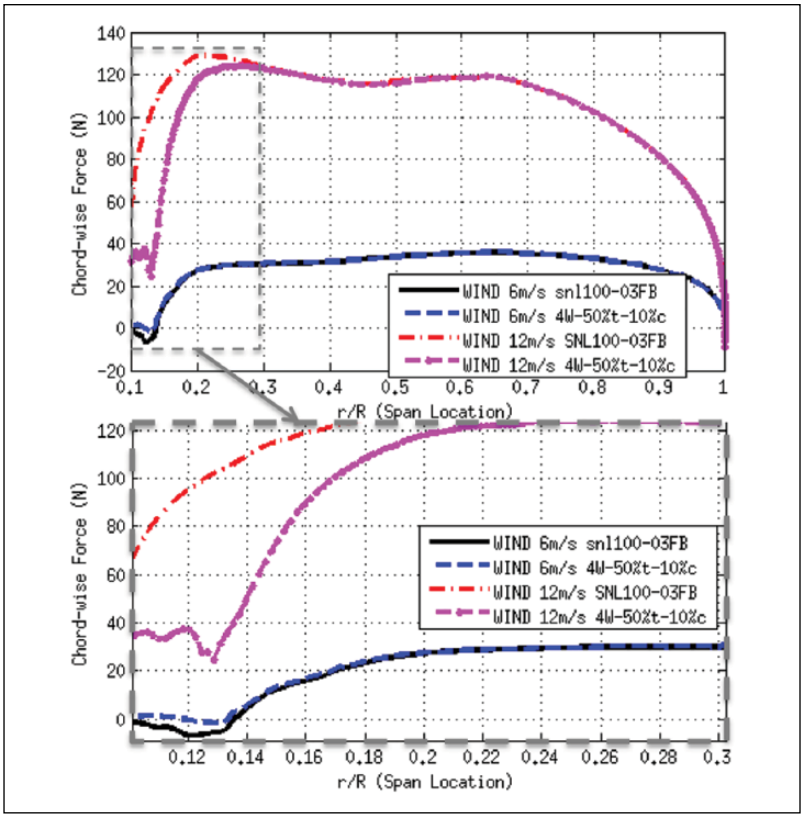

Figure 20. Chord-wise force distribution (in plane) over the blade span.

To figure out the effect of the trailing edge vortex structure variance on the acoustic behavior, time history of the pressure fluctuations is measured behind the turbine blade. The measurement locations are taken at total five points along the radial direction (three points at the blade inboard, and one each points at the mid-span and outboard regions) and 45° behind the blade in the azimuthal direction. The acoustic measurement has been carried out for 900° of blade rotation (2.5 revolutions), with sampling rate of $0.001\,s^{-1}$. In the current study, the sound pressure level has been calculated under the reference sound pressure in air, 20 μPa. Measured acoustic results are shown in Figures 24 and 25. The time histories of the pressure fluctuation are presented in Figure 24, and fast Fourier transformation (FFT) results of the measured acoustic data are shown in Figure 25. High magnitude noise mostly appeared at low frequency ranges (less than 10 Hz). At the location of 0.163 r/R (L1), the modified blade is quieter than the baseline blade at around 5–20 Hz, also at lower frequency range between 1 and 3 Hz. In the pressure fluctuation history, several tonal peaks are observed at the inboard locations, L1, of the baseline blade. Also similar fluctuation peaks are observed in the modified blade case, but weaker and less frequent than the baseline case in general. At the location L3, the power densities of the noise are almost identical between the two blades, except tonal noises of the modified blade at the frequency between 3 and 4 Hz. However, those magnitudes are much lower than the magnitude of the locations L1 and L2. At the mid-span (L4) and the outboard (L5) locations, acoustic noise is linearly decaying at higher frequency ranges, similar at the L3 location.

Test of different sizes of wavy design

The previous results of the "4W-50%t-10%c" trailing edge design resulted on only small variations of aerodynamic and aeroacoustic behaviors. In this section, several bigger wave designs have been investigated. Rather than the last 10% of chord modification, 30% and 50% of chord wavy trailing edge have been selected. The three different wavy tailing edge designs used in the current cases are shown in Figure 26. The current simulations are performed with wind speed of 11.3 m/s. This is the highest wind speed without blade pitch control. The integrated power performance is shown in Table 3. Comparing to the baseline blade, "4W-50%t-10%c" and "4W-50%t-30%c" blades generated slightly lower thrust and power (less than 1%). The "4W-50%t-50%c" blade provided larger thrust and power than the baseline blade although, less than 1% of the total thrust and power. This does not match with the findings of the previous parametric study cases

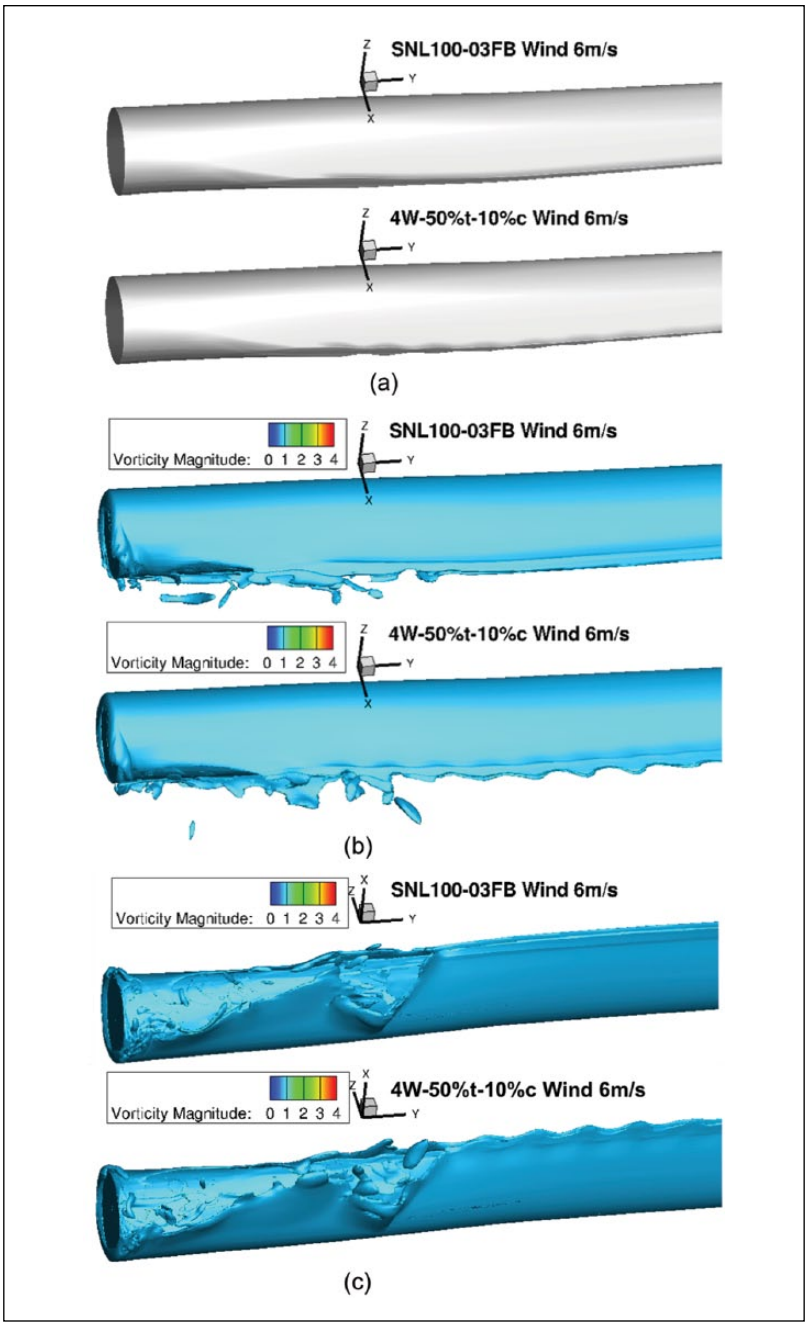

Figure 21. Iso-vorticity magnitude at the blade inboard: wind speed of 6 m/s: (a) geometry, (b) upper surface view, and (c) lower surface view.

which have been performed without the blade rotating. The increase of aerodynamic force in the two wavy trailing edge cases is shown in sectional force distributions over the blade span in Figures 27 and 28. In the axial force distributions, thrust increased at two span locations: ranges of 0.15 r/R through 0.20 r/R and the ranges of 0.10 r/R through 0.12 r/R by the wavy trailing edge modification regardless of the wave size. Tendency of torque distributions is similar to the thrust; however, for "4W-50%t-30%c" generated force is larger from the root to the 0.14 r/R location, but lower than the other blade beyond the location. In contrast, "4W-50%t-50%c" blade generated the highest torque from the 0.16 r/R through the mid-span.

Iso-vorticity contours near the blade inboard are shown in Figure 29. For the baseline blade, flow separation is observed broadly from the root to the 0.2 r/R. Similar patterns of flow separation are also observed in the case of the "4W-50%t-10%c," but the vortex structures are now more regular and circular rather than the irregular structures

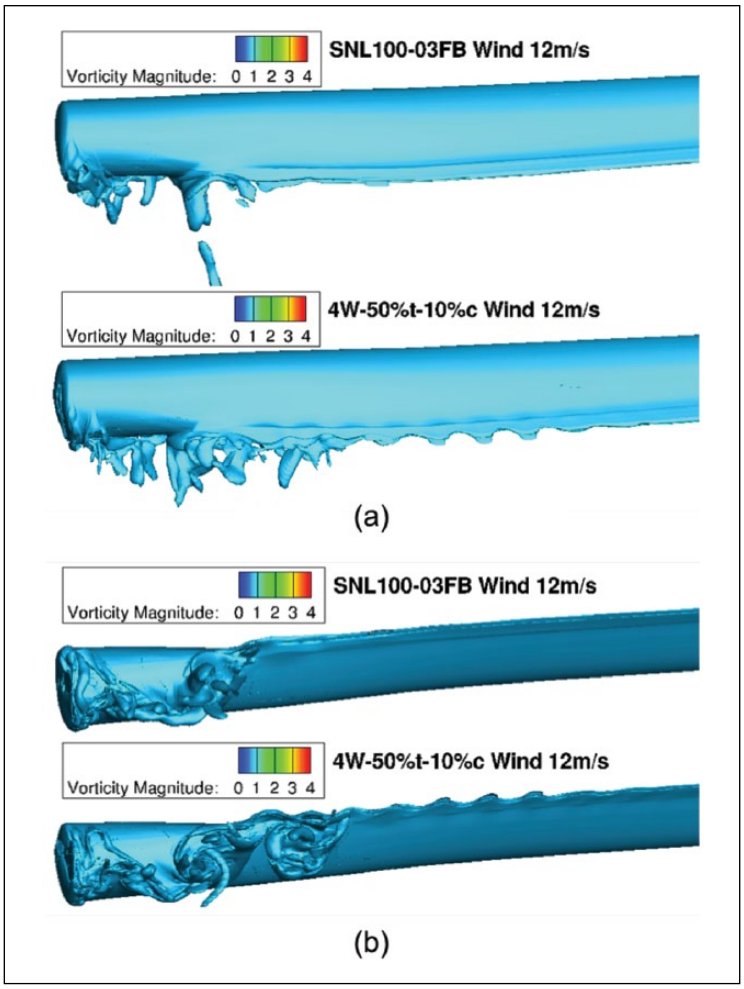

Figure 22. Iso-vorticity magnitude at the blade inboard: wind speed of 12 m/s: (a) upper surface view and (b) lower surface view.

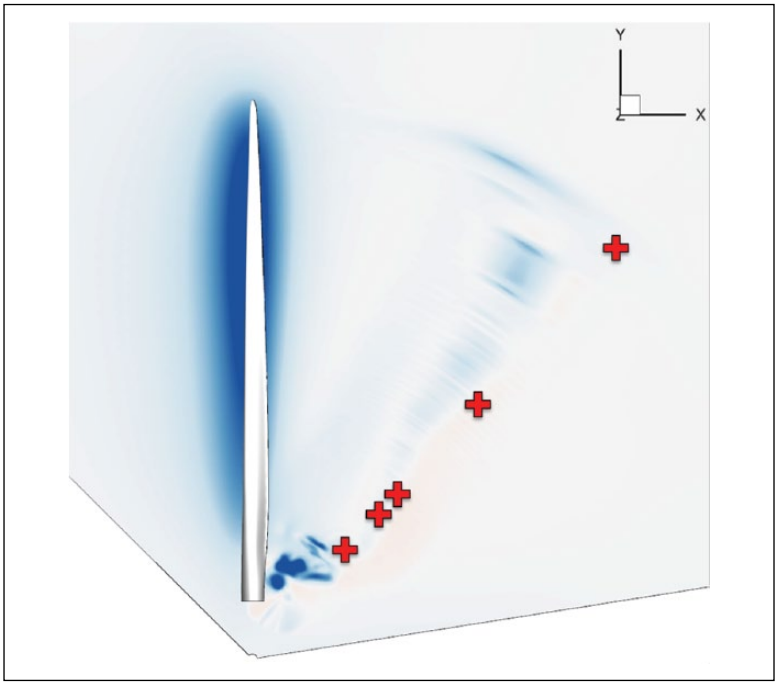

Figure 23. Acoustic pressure measurement locations.

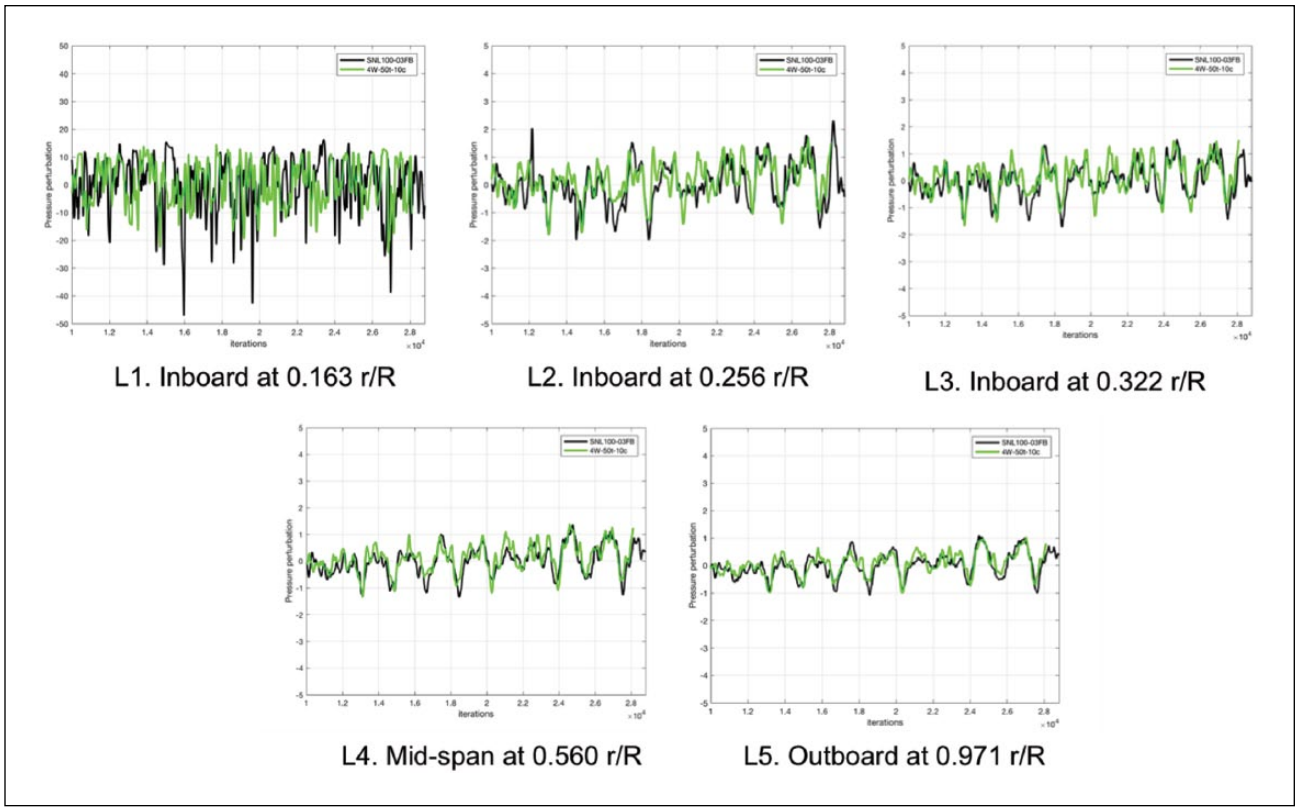

Figure 24. Pressure fluctuations with wind speed of 12 m/s measured behind the turbine blade.

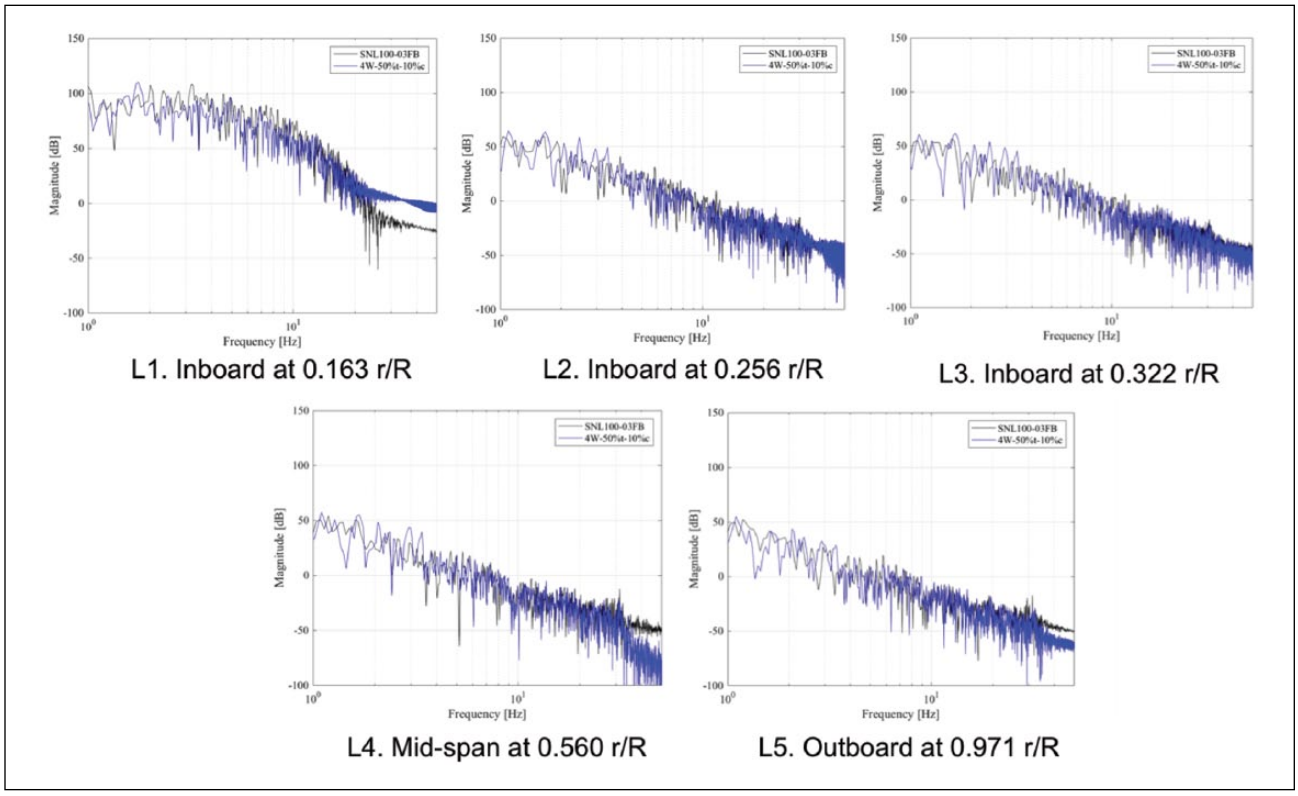

Figure 25. Acoustic behaviors with wind speed of 12 m/s measured behind the turbine blade.

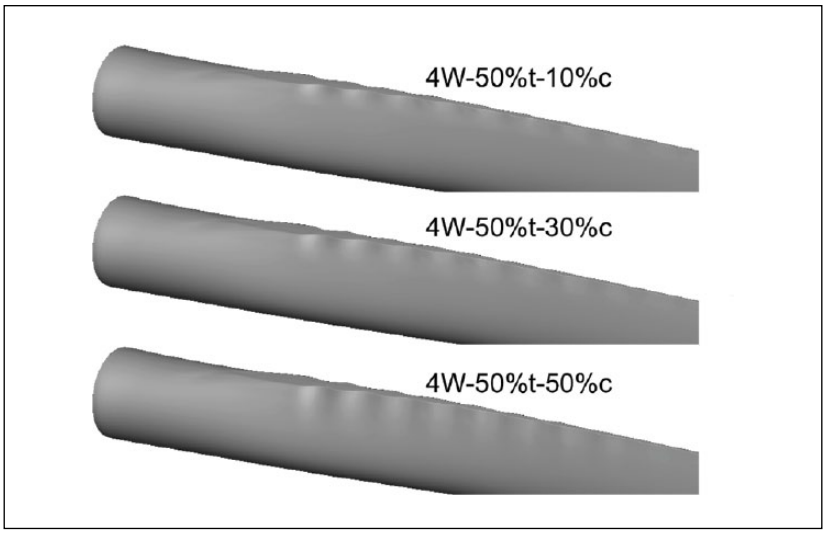

Figure 26. Span-wise wavy trailing edge blades with three different wave sizes: 10%c, 30%c, 50%c.

Table 3. Comparison of power generation between different wavy trailing edge modifications.

Modification type	Thrust (kN)	ΔT	Power (MW)	ΔP
At wind speed of 11.3 m/s				
SNL100-03FB	1862.7	N/A	14.71	N/A
4W-50%t-10%c	1855.5	−0.4%	14.68	−0.2%
4W-50%t-30%c	1862.4	−0.002%	14.68	−0.2%
4W-50%t-50%c	1870.9	+0.44%	14.78	+0.47%

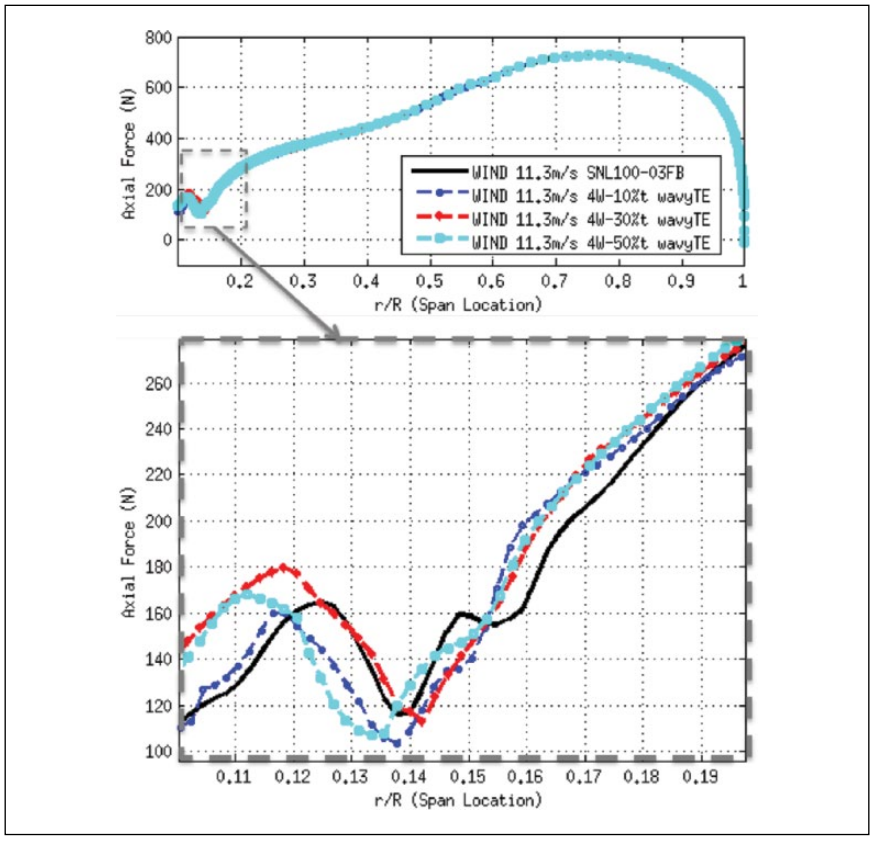

Figure 27. Axial force distribution (out of plane) over the blade span with different sizes of wavy trailing edge: wind speed of 11.3 m/s.

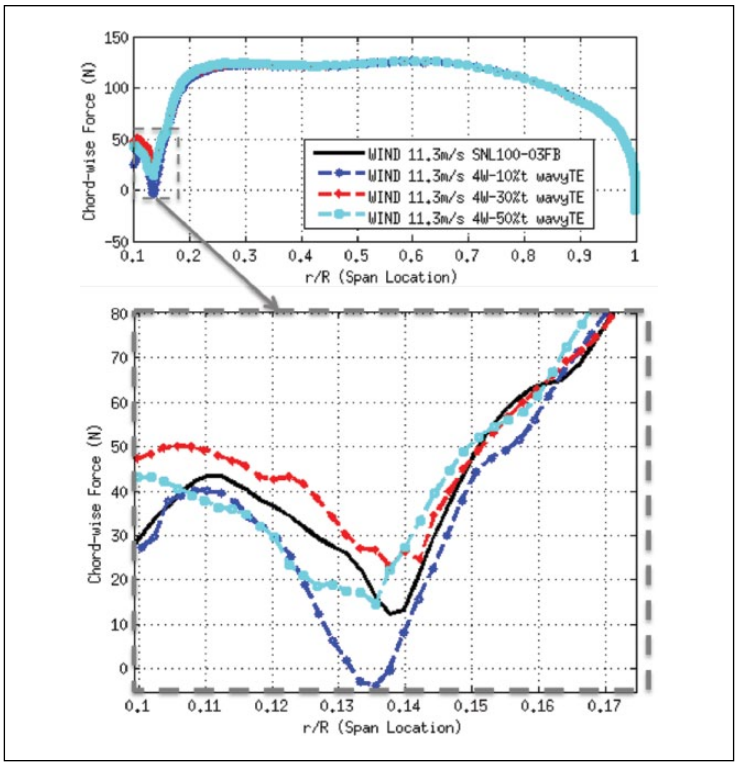

Figure 28. Chord-wise force distribution (in plane) over the blade span with different sizes of wavy trailing edge: wind speed of 11.3 m/s.

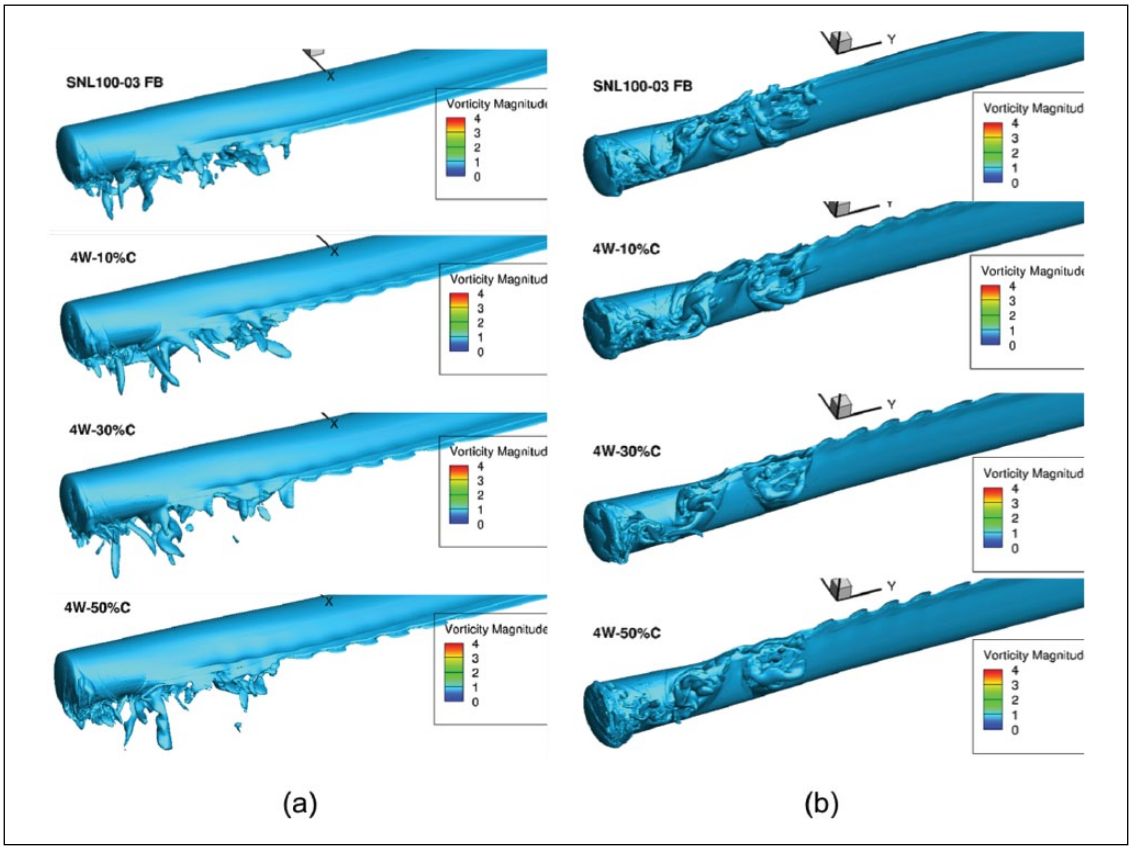

Figure 29. Iso-vorticity magnitude at the blade inboard with different sizes of wavy trailing edge: wind speed of 11.3 m/s: (a) upper surface view and (b) lower surface view.

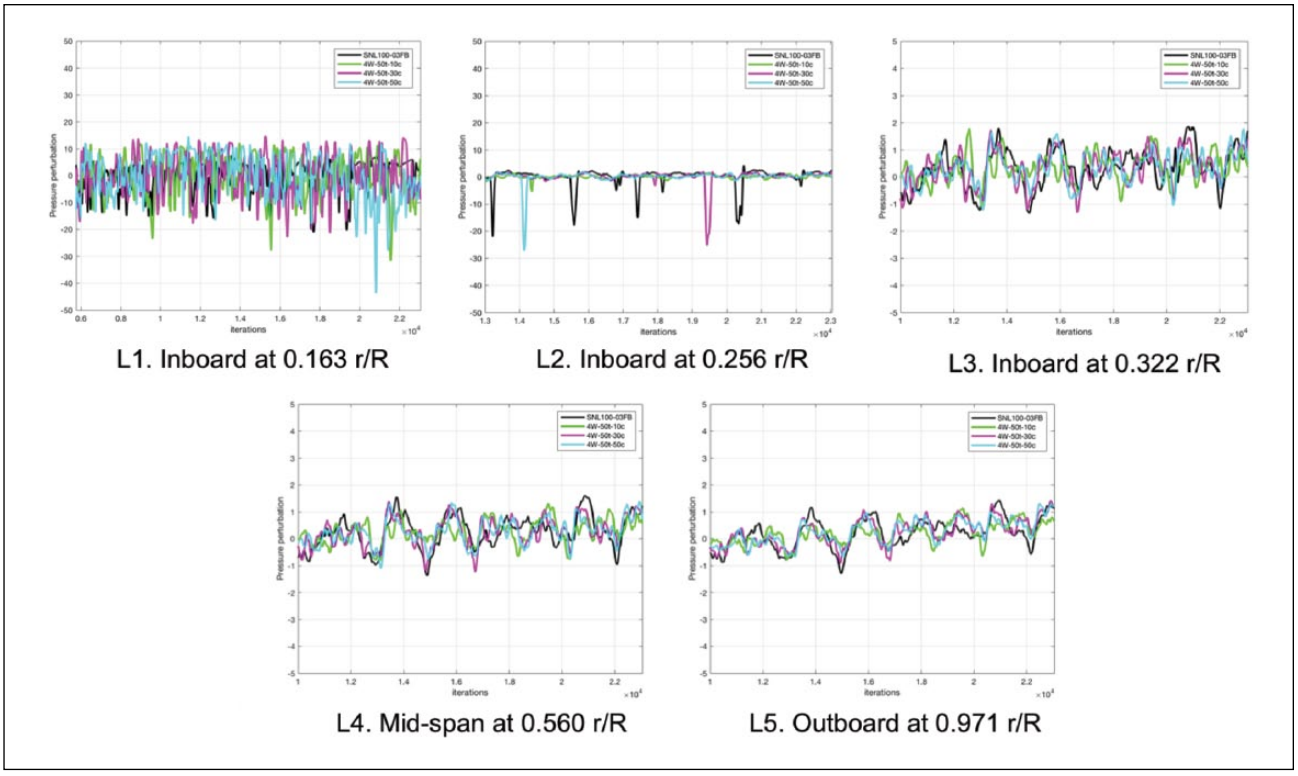

Figure 30. Pressure flucturations of different sizes of wavy trailing edge: wind speed of 11.3 m/s measured behind the turbine blade.

of the baseline case. For the bigger wave cases, flow separation near the root also exists, but now an attached flow region appears between the two separated flow regions. The flow separation at 0.14 r/R also appears for both bigger wave cases, but the vortex structures are much more irregular compared to the clearly circular vortex structures of the "4W-50%t-10%c" result.

Aeroacoustic behaviors depending on the wave size of the modified trailing edge are investigated next. Locations and data sampling rates of acoustic pressure measurement are the same as described in the previous section. The time history of the pressure fluctuation at the measurement locations is plotted in Figure 30. At the wind speed of 11.3 m/s, near the root(L1) location, strong disturbances occurred in all the cases, but mostly stronger with the wavy trailing edge modified blades. However, at the L2 location, the magnitude of the fluctuation peaks was reduced by the wavy modification compared to the baseline blade. The FFT results of the acoustic data are presented in Figure 31. In the plots, the acoustic behaviors between the L1 and L2 points are very different. Based on the results, the wavy trailing edge modification increases the acoustic noise at the blade root (L1), up to 12 dB at a range of frequency 3–10 Hz. However, at the 0.256 r/R (L2), the noise decreases about 50 dB with frequencies of less than 20 Hz, particularly, with the "4W-50%t-10%c" and "4W-50%t-50%c" modifications. These might still be a higher noise level than desired, but the noise level is now similar to that outboard. This is an encouraging outcome. The "4W-50%t-30%c" modification reduced acoustic noise also between 10 and 20 Hz, but is still much louder than the other two modified blades. This tendency is similar to the axial and chord-wise force generation shown in Figures 27 and 28. At the blade inboard, "50%c" wavy modification increases the power generation due to more attached flow on the pressure side of the blade, as shown in Figure 29. This locally attached flow increases rotor thrust, but also acoustic noise level.

Discussions and conclusion

The effect of the span-wise wavy trailing edge on the flatback airfoil wind turbine blade has been investigated using CFD analysis. To provide better understanding of the span-wise wavy trailing edge design parameters, a parametric study of the wave sizing factors has been performed. Two major sizing factors, wave length and depth, have been examined. Consequently, a total of 12 wavy trailing edge patterns have been designed. Based on the results, depth of wave is more dominant to the lift than length of wave. As the wave depth is shallow enough (wave depth/TE thickness < 0.25),

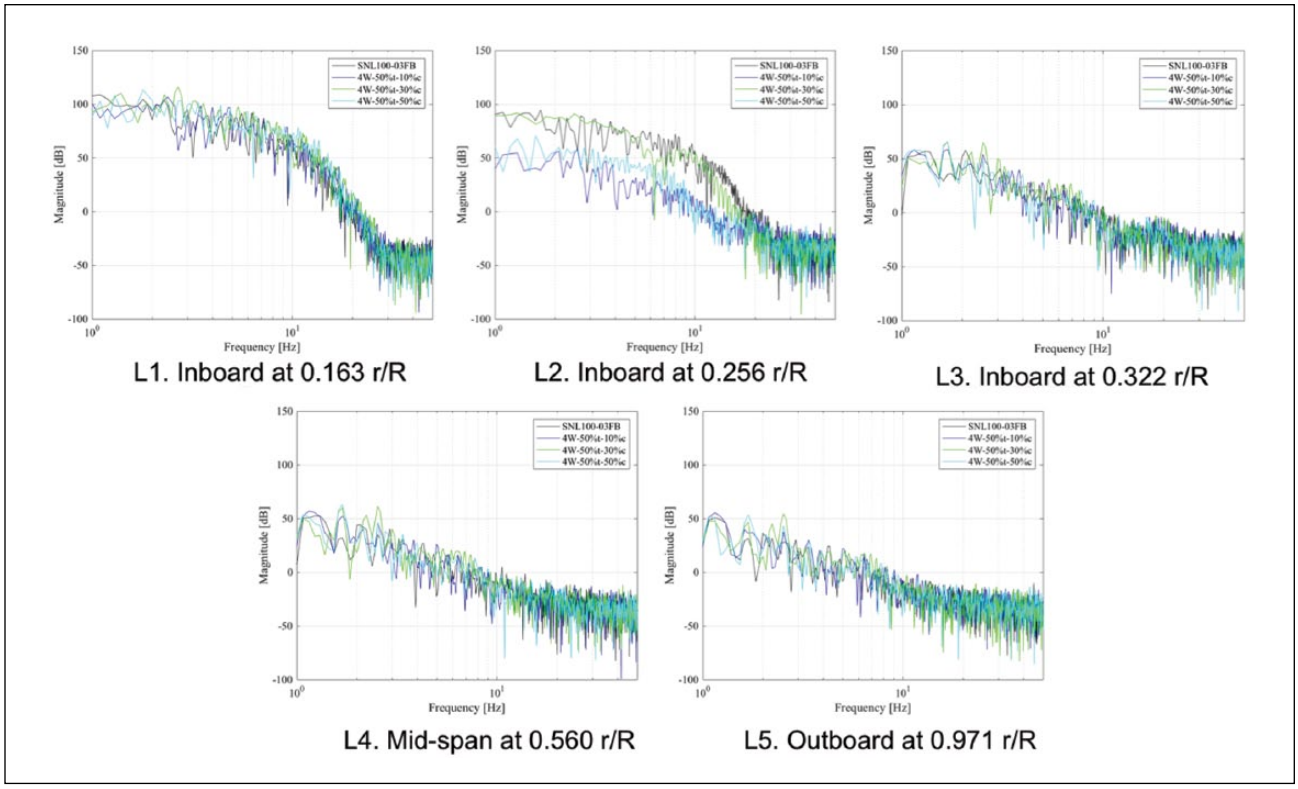

Figure 31. Acoustic behaviors of different sizes of wavy trailing edge: wind speed of 11.3 m/s measured behind the turbine blade.

the lift does not change much no matter how much the length of the wave changes. It is also same for the cases of wave depth/TE thickness, 0.5. However effect of the wave length is much stronger for the wave depth/TE thickness is deeper than 0.75. In contrast of the effect on the lift, the drag is sensitive to both length and depth of wave. The drag reduces when the depth of wave gets deeper and the length of wave gets longer. But, there is a saturation point of the drag reduction in the length of wave variations. The drag is reduced as the length of wave gets longer until the wave length/chord is 0.25, and beyond 0.25, the drag is nearly the same as when the wave length/chord is 0.25.

With considerations of the structural effect of the span-wise wavy trailing edge designs, four additional wavy modified airfoils were created and investigated. Much less portion of the trailing edge (only last 10% of chord) has been modified in these additional geometries, but the modified airfoil such as "FB3500-4W-75%t-10%c" reduces the drag very efficiently and reduces the acoustic noise as well. This is encouraging in a view of structural design issues, because now it is seen that there is no need to vary the blade structure too much, but requires only a minimal portion of the blade structure modification at the trailing edge. To verify structural effect of the span-wise wavy trailing edge designs, a simple eigen buckling simulation has been performed via NuMad design too and Ansys APDL solver. Based on the test results, blade deflections of both baseline and modified blade are almost identical and the lowest mode buckling occurred beyond mid-span region where the third shear web ended rather than the modified locations.

For the rotating blade simulations, the SNL100-03FB blade has been selected as a baseline blade, since the blade contains flatback trailing edge in the inboard region. First, the less portion modification design, "4W-50%t-10%c," has been tested in a range of wind speeds from 4 to 15 m/s. Most of the CFD cases provided slightly under-predicted power generation compared to the BEM results, but within the reasonable ranges. At the lower wind speeds, overall power predictions are not very different between the two blades. However, at the higher wind speeds (specifically for wind speeds require blade pitch controls), the wavy trailing edge causes more flow separation, and the trailing edge vortex shedding is much weaker and its structure is less coherent in span direction. This effect resulted in about 2% of loss of the total power generation, but reduced acoustic noise level at the blade inboard. To verify the effect of wave size of the modification on rotating blade case, larger portion of wavy modified designs, "4W-50%t-30%c" and "4W-50%t-50%c," have been tested at wind speed of 11.3 m/s. In this case, power loss caused by the wavy trailing edge gets recovered as the modified portion of the blade gets bigger, because of the attached flow at the inboard. The attached flow might be related to the formation of trailing edge vortex structure at r/R = 0.14. Based on the results in Figure 29, it indicates that the vortex generated by

root separation becomes stronger at the boundary of the attached flow region, and this may be the source of strong noise peak measured at point L1. In the meanwhile, the circular vortex structures of the modified blades reduced the acoustic noise about 50 dB. The formation of the circular vortex structures is also found in the previous parametric study cases, and shown in Figure 1. In the current result, the ranges of dominant frequency of the acoustic noise are less than 20 Hz. These frequencies may not be audible to human beings, but still affect the human body. In addition, these low frequency noise can affect sea mammals which communicate with low frequency sounds, such as whales. In this sense, the noise reduction by the span-wise wavy trailing edge in the current study is encouraging.

In the current study, it is revealed that one can modify the flatback trailing edge turbine blade to be quieter by the span-wise wavy trailing edge design. However, the amount of variances was less than expected in most cases. This means better optimized wave design is required to use in the real turbine designs. Although we have better understanding of the wavy trailing edge design from the current parametric study, there are other factors that should be considered. The major difference of the design factor between the FB3500 flatback airfoil case and the SNL blade case might be the ratio of trailing edge and airfoil thickness. Further studies, such as design optimization, might be a good idea to improve the design performance of the modification.

Acknowledgements

Current study has been performed using the Deep Thought II cluster at the University of Maryland and the Bluecrab cluster at Johns Hopkins University.

Declaration of conflicting interests

The author(s) declared no potential conflicts of interest with respect to the research, authorship, and/or publication of this article.

Funding

The author(s) received no financial support for the research, authorship, and/or publication of this article.

References

Baker J, Mayda E and van Dam CP (2006) Experimental analysis of thick blunt trailing edge wind turbine airfoils. *Journal of Solar Energy Engineering* 128: 422–431.

Griffith D and Richards P (2014) *The SNL100-03 blade: Design studies with flatback airfoils for the Sandia 100-meter blade*. SAND2014-18129, September. Albuquerque, NM: Sandia National Laboratories.

Koren B (1993) A robust upwind discretization method for advection, diffusion and source terms. Braunschweig. Vieweg: 118 ISBN 3-528-07645-3.

Medida S and Baeder JD (2011) Application of the correlation-based $\gamma - \overline{Re_{\theta t}}$ transition model to the Spalart-Allmaras Turbulence Model. In: *20th AIAA computational fluid dynamics conference*, Honolulu, HI, 27–30 June.

Roe PL (1981) Approximate Riemann Solvers, Parameters Vectors, and Difference Schemes. *Journal of Computational Physics* 43: 357–372.

Spalart PR, Deck S, Shur ML, et al. (2006) A new version of detached eddy simulation, resistant to ambiguous grid densities. *Theoretical Computational Fluid Dynamics* 20: 181–195.

Stone C, Barone M, Eric Lynch E, et al. (2009) A computational study of the aerodynamics and aeroacoustic of a flatback airfoil using hybrid RANS-LES. In: *AIAA 47th aerospace sciences meeting and exhibit*, Orlando, FL, 5–8 January, paper no. AIAA-2009-0273.

Thomas S and Baeder JD (2013) Modeling the two-phase flowfield beneath a hovering rotor on graphics processing units using a FVM-RANS hybrid methodology. In: *21st AIAA computational fluid dynamics conference*, San Diego, CA, 24–27 June.

Turkel E (1987) Preconditioned Methods for Solving the Incompressible and Low Speed Compressible Equations. *Journal of Computational Physics* 72: 277–298.

Van Dam CP, Kahn D and Berg D (2008) *Trailing edge modifications for flatback airfoils*. SAND2008-1781, March. Albuquerque, NM: Sandia National Laboratories.

Van Leer B (1979) Towards the ultimate conservative difference scheme. V. A second-order sequel to Godunov's method. *Journal of Computational Physics* 32(1): 101–136.

Yang SJ and Baeder JD (2015) Aerodynamic drag and aeroacoustic noise mitigation of flatback airfoil with spanwise wavy trailing edge. In: *AIAA Scitech 2015*, Kissimmee, FL, 5–9 January.

Yang SJ and Baeder JD (2016) Effect of wavy trailing edge on 100meter flatback wind turbine blade. *Journal of Physics: Conference Series* 753: 022060.

Yoon S and Jameson A (1988) Lower-Upper Symmetric-Gauss-Seidel Method for the Euler and Navier-Stokes Equations. *AIAA Journal* 26(9): 1025–1026.